Geomechanics and Engineering, *Vol. 43, No. 3 (2025) 197-211*
https://doi.org/10.12989/gae.2025.43.3.197

Pseudo-dynamic analysis of asymmetric collapse mechanism in shallow tunnels

Jiayun Liang[1,2a], Jie Cui[1,3b], Yadong Li[*1,3], Yi Shan[1,3c], Zhicheng Yang[4d] and Marco Donà[2,5e]

[1]*School of Civil Engineering, Guangzhou University, Guangzhou, 510006, China*
[2]*Guangzhou Pearl River Construction Development CO. LTD., Guangzhou, Guangdong, 510075, China*
[3]*Guangdong Provincial Engineering and Technology Research Center of Geo-Structure Safety and Protection, Guangzhou University, Guangzhou, Guangdong, 510006, China*
[4]*College of Urban and Rural Construction, Zhongkai University of Agriculture and Engineering, Guangzhou, 510225, China*
[5]*Department of Geosciences, University of Padova, Via G. Gradenigo 6, 35131 Padua, Italy*

(*Received October 10, 2023, Revised October 19, 2025, Accepted October 20, 2025*)

Abstract. In order to solve the collapse failure problem of overlying rock mass in shallow tunnels during earthquake, and to guide the design of tunnels safety width and the reinforcement of overlying rock mass, the prediction method of collapse failure curve under earthquake is studied. The main means is to simulate the seismic wave action on the overlying rock mass by the pseudo-dynamic method, establish the virtual power equation in the upper bound theorem based on the Hoek-Brown criterion, and solve it by the variational method of the variable endpoint problem. The effects of seismic wave parameters, rock mass strength parameters and engineering parameters on the predicted collapse area are analysed. The results show that the horizontal seismic acceleration affects the shape of the collapsing rock block, while the vertical seismic acceleration affects the size; the rock mass with weak strength and high density has a small size of collapsed rock block. By referring to the influence of engineering parameters, reducing the depth of the tunnel and uniform load on the surface and increasing the supporting pressure on the overlying rock mass can help to restrain the occurrence of collapse.

Keywords: asymmetric collapse mechanism; Hoek-Brown failure criterion; psudo-dynamic analysis; shallow tunnels; upper bound theorem; variational method

1. Introduction

Among various engineering vibration problems (Kwak *et al*. 2024, Yang *et al*. 2025), seismic damage to tunnels has been attracting considerable attention from both research and engineering communities (Azadi *et al*. 2020, Xue *et al*. 2020, Zhang *et al*. 2020). Earthquake damage to tunnel has been studied (Wang *et al*. 2001, Wang *et al*. 2009, Jiang *et al*. 2010), and it is found that the tunnel portal is one of the most concentrated sections of tunnel damage, with various damage patterns. One of the damage patterns is the collapse of the tunnel roof lining and overlying surrounding rock near the tunnel portal. In order to prevent the tunnel portal from being damaged by collapsed rock mass, it is necessary to study the collapse mechanism of overlying rock mass.

At present, there are few theoretical studies on seismic collapse mechanism of overlying rock mass at tunnel portal, while the analytical solution of static collapse curve of overlying rock mass at shallow tunnel has been proposed by several scholars. Fraldi and Guarracino (2009, 2010, 2011) proposed that the rock mass overlying the deep tunnel will collapse when the internal stress of the rock mass reaches the failure strength due to gravity action. They combined the upper bound theorem and Hoek-Brown criterion to obtain the curve of failure in rock mass, which is the boundary of the block that's about to collapse. It regards the collapsing block as rigid, so it prevents the rock from collapsing when the tunnel width is smaller than the width of the collapsing rock block. In addition, the collapse can also be prevented by reinforce areas that are predicted to collapse. In order to solve the collapse problem of shallow tunnels, Yang and Huang (2011, 2013) proposed two-dimensional and three-dimensional analytical method of collapse curves for a shallow tunnel according to the analytical methods proposed by Fraldi and Guarracino (2009) (Fig. 1).

Subsequently, the method of calculating the collapse curve of the shallow tunnel has been applied to a variety of stratum conditions. Huang *et al*. (2017) applied the calculation method of the collapse curve of shallow tunnel to the problem of deep tunnel with cave above. Wang *et al*. (2019), Qin *et al*. (2017, 2018) and Guo *et al*. (2021) used the calculation method of Yang and Huang (2011) to study the collapse mechanism of shallow tunnel in multiple rock layers. Lyu (2019) put forward an analytical method for the asymmetrical collapse mechanism of the tunnel in inclined

*Corresponding author, Professor
E-mail: liyadong@gzhu.edu.cn
[a]Postdoctoral Fellow
[b]Professor
[c]Associate Professor
[d]Associate Professor
[e]Professor

ISSN: 2005-307X (Print), 2092-6219 (Online)

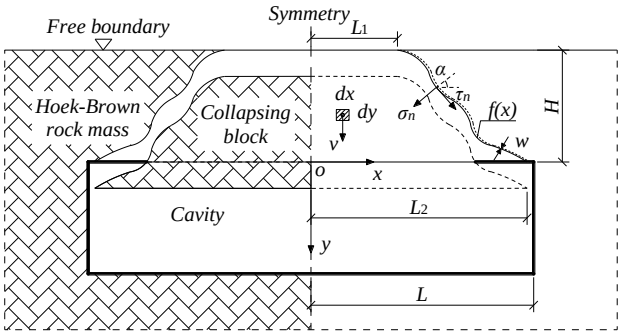

Fig. 1 Collapse mechanism of shallow tunnel (Yang and Huang 2011)

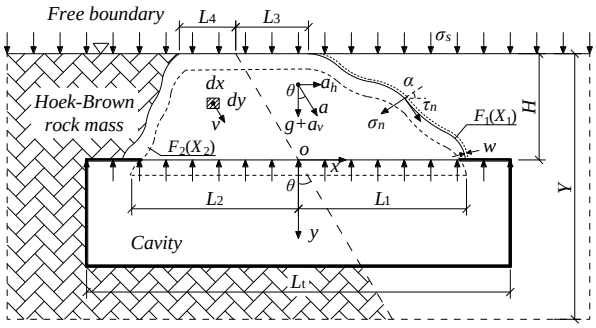

Fig. 2 Asymmetric collapse mechanism of shallow tunnel

rock stratum. But it is still limited to the application of static problems. This is because the variational method of the known endpoint problem is used to solve the problem of the variable endpoint in above articles, which means that the limiting conditions are insufficient. Therefore, the existing theoretical solution of the collapse problem should be optimized (Liang *et al*. 2022a, b).

In addition, in order to apply the complex seismic action to the limit analysis of the collapse problem, the pseudo-dynamic method, which is widely used in the field of geotechnical engineering, is used to simplify the seismic action. The pseudo-dynamic method, originally proposed by Steedman and Zeng (1990), defines the shear wave as a sine wave function considering the amplification factor. Choudhury and Nimbalkar (2006) took into account the combined effects of longitudinal waves and improved the pseudo-dynamic analysis. Zhang *et al*. (2017, 2021) and Huang *et al*. (2021) have applied the pseudo-dynamic method to the study of tunnel working face stability. In this study, the collapse model considering the combined action of longitudinal wave and shear wave is shown in Fig. 2.

Therefore, the aim of the analytical study is to solve the expression of the collapse curve of overlying rock mass under the combined action of longitudinal wave and shear wave by using the variational method of variable endpoints, based on the pseudo-dynamic method and upper bound theorem.

2. Method of analysis

The main analysis method of this study is to set up the virtual power equilibrium equation according to the upper bound theorem and Hoek-Brown strength criterion, and to solve the virtual power equilibrium equation by the variational method to obtain the collapse curve expression. The assumptions and main analysis methods are introduced in the following.

2.1 Assumption

The expressions of horizontal acceleration $a_h(y, t)$ and vertical acceleration $a_v(y, t)$ in pseudo-dynamic analysis of retaining wall problem are (Choudhury and Nimbalkar 2006)

$$a_h(y,t)=\left[1+\frac{Y-y}{Y}\left(f_k-1\right)\right]k_h g\sin\left[\omega\left(t-\frac{Y-y}{v_s}\right)\right] \quad (1)$$

$$a_v(y,t)=\left[1+\frac{Y-y}{Y}\left(f_k-1\right)\right]k_v g\sin\left[\omega\left(t-\frac{Y-y}{v_p}\right)\right] \quad (2)$$

where Y is the retaining wall height; y is the value of the y-coordinate; f_k is the amplification factor; k_h and k_v are horizontal and vertical acceleration coefficients respectively. ω is angular frequency of base shaking, $\omega = 2\pi f$, where f is frequency. v_s is shear wave velocity, $v_s = (G/\rho)1/2$,and v_p is longitudinal wave velocity, $v_p = [2G(1-\upsilon)/\rho(1-2\upsilon)]1/2$,where G is shear modulus; ρ is density of soil or rock; υ is poisson's ratio. Some assumptions need to be set to make the pseudo-dynamic analysis suitable for tunnel collapse: 1) Seismic waves are transmitted from the bottom of the rock stratum, i.e., Y is the thickness of the rock stratum; 2) For simplicity, ignoring the effects of tunnels on seismic waves; 3) Since the depth y near the surface has almost no effect on the seismic acceleration in this study, $y = 0$ can be set.

The magnitude of the resultant acceleration, $g_a(t)$, is

$$g_a(t)=\left[g+a_v(t)\right]\cos\theta+a_h(t)\sin\theta \quad (3)$$

which is made up of gravity acceleration g, vertical seismic acceleration $a_v(t)$ and horizontal seismic acceleration $a_h(t)$. And the angle θ between $g_a(t)$ and y-axis are calculated by

$$\theta=\arctan\left\{a_h(t)\left[g+a_v(t)\right]^{-1}\right\} \quad (4)$$

It should be noted that assumption 2) may lead to an underestimation of the seismic acceleration. In reality, the presence of the tunnel exhibits an amplification effect on seismic waves (Zhu *et al.* 2024, Abdelhalim *et al.* 2025). It is therefore recommended that, in engineering practice, an amplification factor be introduced into Eqs. (1) and (2) to account for the actual conditions.

In the study of Yang and Huang (2011), since the failure of the boundary of the collapsing block is only caused by its gravity, the geometry and mechanical state of the collapsing block are symmetric along the y-axis (Fig. 1). Therefore, half of the collapsing block divided along the y-axis satisfy the virtual power equation. When the combined action of shear wave and longitudinal wave is considered, the

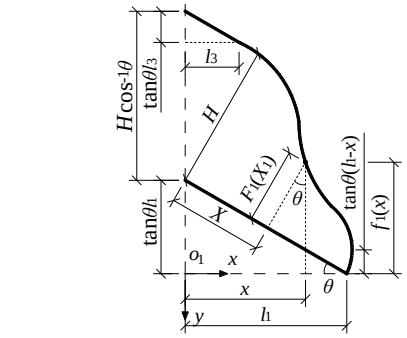

(a) xo_1y coordinate system

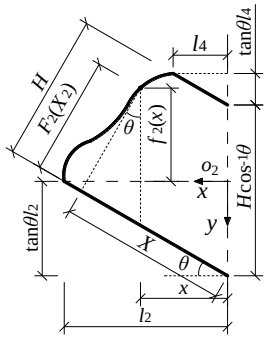

(b) xo_2y coordinate system

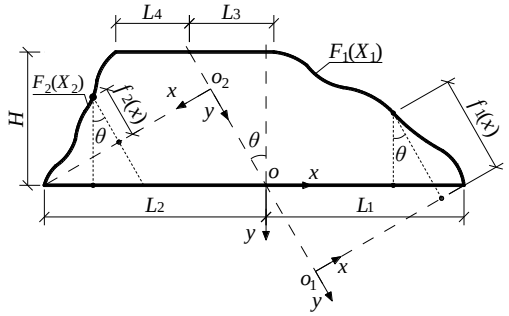

(c) xoy coordinate system

Fig. 3 The geometrical relation between xoy, xo_1y and xo_2y coordinates

collapsing block is only affected by the resultant acceleration $g_a(t)$. Similarly, an axis in the direction of $g_a(t)$ can be found to divide the collapsing block and both sides of the rock block respectively satisfy the virtual power equation. And the two parts of the collapsing rock block can be regarded as independent research objects.

Since the position relationship between the collapsing block and $g_a(t)$ axis is unknown, the position of $g_a(t)$ axis can be assumed first, that through the origin of xoy coordinate system (Fig. 2). And new coordinate systems xo_1y and xo_2y are built for the two parts of the collapsing block (Figs. 3(a)-(b)). The collapse curves $F_1(X)$ and $F_2(X)$ and the widths L_i (i = 0, 1, 2, 3) in the xoy coordinate system can be represented by $f_1(x)$, l_1 and l_3 in the xo_1y coordinate system and $f_2(x)$, l_2 and l_4 in the xo_2y coordinate system, respectively (Fig. 3).

2.2 Energy analysis and variational solution

The upper bound theorem of limit analysis is a method to determine the approximate maximum solution of deformation load, by combining the principle of virtual work and the principle of maximum dissipation work. In other words, the minimum volume can be calculated when the internal force of the collapsing block boundary reaches the ultimate failure. The generalized expression of virtual power equation is shown in Eq. (5) (Chen 1975, 1990).

$$\int_S T_i v_i^* dS + \int_V F_i v_i^* dV = \int_V \sigma_{ij} \dot{\varepsilon}_{ij}^* dV \tag{5}$$

where T_i and F_i are external forces on the surface and body forces; v_i* is virtual velocity of kinematically admissible velocity field; S is the surfaces of external forces; V is the volume of the body; and are stresses and strain rate of deformations, compatible with the external forces T_i on the surface and with F_i in the body. The surface force acting on the collapsing rock mass consists of support pressure and uniformly load on the surface, as shown in Fig. 2. And based on the hypothesis in Section 2.1, the expressions of physical force are the functions of $f_1(x)$ and $f_2(x)$, and the internal stresses are defined by Hoek-Brown strength criterion.

Hoek-Brown criterion is used to estimate rock strength based on rock strength test data and engineering experience (Hoek *et al*. 1997, 2002, 2018). Its generalized expression is

$$\sigma_1 = \sigma_3 + \sigma_{ci}\left(m_b \frac{\sigma_3}{\sigma_{ci}} + s\right)^a \tag{6}$$

where σ_1 and σ_3 are the maximum and minimum effective stresses at failure respectively; σ_{ci} is the uniaxial compressive strength and is derived from the strength test; m_b is given by

$$m_b = m_i e^{\frac{GSI-100}{28-14D}} \tag{7}$$

s and a are constants for the rock mass and are defined as

$$s = e^{\frac{GSI-100}{9-3D}} \tag{8}$$

$$a = \frac{1}{2} + \frac{1}{6}\left(e^{-GSI/15} - e^{-20/3}\right) \tag{9}$$

The Geological Strength Index GSI, material constant m_i and disturbance factor D are defined by Hoek-Brown criterion based on rock mass strength. The Geological Strength Index GSI and disturbance factor D are estimated empirically, material constant mi is derived from strength tests. Since Eq. (6) can be converted to the expression of Mohr-Coulomb criterion, Hoek-Brown criterion can be applied to estimate the rock mass strengths over the complete range of rock mass types, including different and problematic rock masses.

Since the shape of the collapsing block is not known, the correlation between the collapse curve and the principal stresses in Eq. (6) cannot be established. Consequently, the analysis proceeds with the equivalent Mohr envelope

$$\tau_n = A\sigma_{ci}\left(\frac{\sigma_n - \sigma_t}{\sigma_{ci}}\right)^B \tag{10}$$

where σ_n and τ_n are the normal and tangential stresses of rock mass when it reaches ultimate failure; σ_t is tensile strength; A and B are the constants of the material, which are obtained by fitting the triaxial test results. The details of converting the Hoek-Brown criterion to the equivalent Mohr envelope are provided in Appendix A. Since the two cannot be completely equivalently transformed, the methods for determining the values of A, B, and σ_t need to be considered (Suchowerska *et al*. 2012, Park 2023, 2025).

When the rock block begins to collapse, the internal force at the boundary of the collapsing block reaches the mechanical state of Hoek-Brown failure criterion. Based on Eq. (10), the expressions of internal energy dissipation rate on collapse curve $f_1(x)$ and $f_2(x)$ are listed in Eqs. (11) and (12) respectively, and their derivation process is referred to the article published by Fraldi and Guarracino (2009).

$$\dot{D}_{i1}=\sigma_{ij,1}\dot{\varepsilon}^{*}_{ij,1}= \left[\sigma_{ci}A^{\frac{1}{1-B}}(B-1)B^{\frac{B}{1-B}}f_1'(x)^{\frac{1}{1-B}}-\sigma_t\right]\left[1+f_1'(x)^2\right]^{-\frac{1}{2}}\frac{v}{w} \tag{11}$$

$$\dot{D}_{i2}=\sigma_{ij,2}\dot{\varepsilon}^{*}_{ij,2}= \left[\sigma_{ci}A^{\frac{1}{1-B}}(B-1)B^{\frac{B}{1-B}}f_2'(x)^{\frac{1}{1-B}}-\sigma_t\right]\left[1+f_2'(x)^2\right]^{-\frac{1}{2}}\frac{v}{w} \tag{12}$$

where v is virtual velocity; w is the width at which plastic deformation occurs in the rock mass. Since Fraldi and Guarracino (2009) assumes that the collapsing rock block is rigid, plastic deformation does not occur on the collapsing rock block.

As shown in Figs. 3(a) and 3(b), the body force power of the two parts of the collapse block can be respectively expressed as

$$\dot{W}_1=\int_V F_{i,1}v_i^{*}dV= \rho g_a(t)\left[\int_{l_3}^{l_1}f_1(x)+(x-l_3)\tan\theta dx-l_3H\cos^{-1}\theta\right]v \tag{13}$$

$$\dot{W}_2=\int_V F_{i,2}v_i^{*}dV= \rho g_a(t)\left[\int_{l_4}^{l_2}f_2(x)-(x-l_4)\tan\theta dx-l_4H\cos^{-1}\theta\right]v \tag{14}$$

The expressions of the power of the support pressure and the power of the uniformly load on the surface are shown in Eqs. (15) and (16), which together constitute the power of surface force acting on the collapsing rock block.

$$\dot{P}_{qi}=-qL_i\cos\theta v=-ql_iv,\quad i=1,\ 2 \tag{15}$$

$$\dot{P}_{\sigma_s i}=\sigma_sL_i\cos\theta v=\sigma_sl_iv,\quad i=1,\ 2 \tag{16}$$

$$\int_S T_{i,1}v_i^{*}dS=\dot{P}_{q1}+\dot{P}_{\sigma_s 1} \tag{17}$$

$$\int_S T_{i,2}v_i^{*}dS=\dot{P}_{q2}+\dot{P}_{\sigma_s 2} \tag{18}$$

Based on the assumption that the total dissipation rate of the collapsing block on both sides of the axis is zero, the expression of total dissipation rate can be written as two independent equations

$$\begin{aligned}\dot{\Psi}_1&=\int_V\sigma_{ij,1}\dot{\varepsilon}^{*}_{ij,1}dV+\int_S T_{i,1}v_i^{*}dS-\int_V F_{i,1}v_i^{*}dV\\ &=\int_{l_3}^{l_1}w\dot{D}_{i1}\left[1+f_1'(x)^2\right]^{\frac{1}{2}}dx-\dot{W}_1+\dot{P}_{q1}+\dot{P}_{\sigma_s 1}\\ &=\begin{bmatrix}\int_{l_3}^{l_1}\sigma_{ci}A^{\frac{1}{1-B}}(B-1)B^{\frac{B}{1-B}}f_1'(x)^{\frac{1}{1-B}}-\sigma_t-q_{dx}\\ -\rho g_a(t)f_1(x)-\rho g_a(t)(x-l_3)\tan\theta\\ +\rho g_a(t)l_3H\cos^{-1}\theta+\sigma_sl_3-ql_3\end{bmatrix}v\end{aligned} \tag{19}$$

$$\begin{aligned}\dot{\Psi}_2&=\int_V\sigma_{ij,2}\dot{\varepsilon}^{*}_{ij,2}dV+\int_S T_{i,2}v_i^{*}dS-\int_V F_{i,2}v_i^{*}dV\\ &=\int_{l_4}^{l_2}w\dot{D}_{i2}\left[1+f_2'(x)^2\right]^{\frac{1}{2}}dx-\dot{W}_2+\dot{P}_{q2}+\dot{P}_{\sigma_s 2}\\ &=\begin{bmatrix}\int_{l_4}^{l_2}\sigma_{ci}A^{\frac{1}{1-B}}(B-1)B^{\frac{B}{1-B}}f_2'(x)^{\frac{1}{1-B}}-\sigma_t-q_{dx}\\ -\rho g_a(t)f_2(x)+\rho g_a(t)(x-l_4)\tan\theta\\ +\rho g_a(t)l_4H\cos^{-1}\theta+\sigma_sl_4-ql_4\end{bmatrix}v\end{aligned} \tag{20}$$

Since $\dot{D}_i$ and $\dot{W}$ act in the direction of v but their values are both negative, while T_i is positive, the sign of T_i term is opposite to that of $\dot{D}_i$ and $\dot{W}$.

According to the upper bound theorem, when the minimum value of the total dissipation rate is zero, the expression functions of the collapse curves $f_1(x)$ and $f_2(x)$ can be obtained. The objective functions of the variational calculation are shown in Eqs. (21) and (22).

$$\Lambda_1\left[x,f_1'(x),f_1(x)\right]= \begin{bmatrix}\sigma_{ci}A^{\frac{1}{1-B}}(B-1)B^{\frac{B}{1-B}}f_1'(x)^{\frac{1}{1-B}}-\sigma_t-q\\ -\rho g_a(t)f_1(x)-\rho g_a(t)(x-l_3)\tan\theta\end{bmatrix}v \tag{21}$$

$$\Lambda_2\left[x,f_2'(x),f_2(x)\right]= \begin{bmatrix}\sigma_{ci}A^{\frac{1}{1-B}}(B-1)B^{\frac{B}{1-B}}f_2'(x)^{\frac{1}{1-B}}-\sigma_t-q\\ -\rho g_a(t)f_2(x)+\rho g_a(t)(x-l_4)\tan\theta\end{bmatrix}v \tag{22}$$

Since there is no known condition to define the position of the endpoints of collapse curves $f_1(x)$ and $f_2(x)$, the endpoints are movable during variational calculation. Therefore, when using the variational method to solve the variable endpoints problem, the variational equations are as follows

$$\begin{aligned}\delta\dot{\Psi}_1=&\int_{l_3}^{l_1}\left\{\frac{\partial\Lambda_{f_1}}{\partial f_1(x)}-\frac{\partial}{\partial x}\left[\frac{\partial\Lambda_{f_1}}{\partial f_1'(x)}\right]\right\}\delta f_1(x)dx\\ &+\left[\Lambda_{f_1}-f_1'(x)\frac{\partial\Lambda_{f_1}}{\partial f_1'(x)}-\frac{\partial\Gamma_1}{\partial x}\frac{\partial\Lambda_{f_1}}{\partial f_1'(x)}\right]\Bigg|_{x=l_1}\delta l_1\\ &+\left[\Lambda_{f_1}-f_1'(x)\frac{\partial\Lambda_{f_1}}{\partial f_1'(x)}-\frac{\partial\Gamma_3}{\partial x}\frac{\partial\Lambda_{f_1}}{\partial f_1'(x)}\right]\Bigg|_{x=l_3}\delta l_3=0\end{aligned} \tag{23}$$

$$\delta\dot{\Psi}_2 = \int_{l_4}^{l_2}\left\{\frac{\partial\Lambda_{f_2}}{\partial f_2(x)} - \frac{\partial}{\partial x}\left[\frac{\partial\Lambda_{f_2}}{\partial f_2'(x)}\right]\right\}\delta f_2(x)dx + \left[\Lambda_{f_2} - f_2'(x)\frac{\partial\Lambda_{f_2}}{\partial f_2'(x)} - \frac{\partial\Gamma_2}{\partial x}\frac{\partial\Lambda_{f_2}}{\partial f_2'(x)}\right]_{x=l_2}\delta l_2 + \left[\Lambda_{f_2} - f_2'(x)\frac{\partial\Lambda_{f_2}}{\partial f_2'(x)} - \frac{\partial\Gamma_4}{\partial x}\frac{\partial\Lambda_{f_2}}{\partial f_2'(x)}\right]_{x=l_4}\delta l_4 = 0 \quad (24)$$

where Γ_i (i = 1,2,3,4) represent the trajectories of the corresponding endpoints, and their expressions are as follows

$$\Gamma_1(x,y) = y + \tan\theta(l_1 - x) = 0 \quad (25)$$

$$\Gamma_3(x,y) = y + \tan\theta(l_1 - x) + H\cos^{-1}\theta = 0 \quad (26)$$

$$\Gamma_2(x,y) = y - \tan\theta(l_2 - x) = 0 \quad (27)$$

$$\Gamma_4(x,y) = y + \tan\theta(x - l_2) + H\cos^{-1}\theta = 0 \quad (28)$$

Since $f_1(x)$, $f_2(x)$ and l_i (i = 0,1,2,3) are all undetermined, $\delta f_1(x)$, $\delta f_2(x)$ and δl_i (i = 0,1,2,3) are not zero. Thus, Eqs. (23) and (24) can be simplified into the following 6 equations.

$$\frac{\partial\Lambda_{f_1}}{\partial f_1(x)} - \frac{\partial}{\partial x}\left[\frac{\partial\Lambda_{f_1}}{\partial f_1'(x)}\right] = 0 \quad (29)$$

$$\left[\Lambda_{f_1} - f_1'(x)\frac{\partial\Lambda_{f_1}}{\partial f_1'(x)} - \frac{\partial\Gamma_1}{\partial x}\frac{\partial\Lambda_{f_1}}{\partial f_1'(x)}\right]_{x=l_1} = 0 \quad (30)$$

$$\left[\Lambda_{f_1} - f_1'(x)\frac{\partial\Lambda_{f_1}}{\partial f_1'(x)} - \frac{\partial\Gamma_3}{\partial x}\frac{\partial\Lambda_{f_1}}{\partial f_1'(x)}\right]_{x=l_3} = 0 \quad (31)$$

$$\frac{\partial\Lambda_{f_2}}{\partial f_2(x)} - \frac{\partial}{\partial x}\left[\frac{\partial\Lambda_{f_2}}{\partial f_2'(x)}\right] = 0 \quad (32)$$

$$\left[\Lambda_{f_2} - f_2'(x)\frac{\partial\Lambda_{f_2}}{\partial f_2'(x)} - \frac{\partial\Gamma_2}{\partial x}\frac{\partial\Lambda_{f_2}}{\partial f_2'(x)}\right]_{x=l_2} = 0 \quad (33)$$

$$\left[\Lambda_{f_2} - f_2'(x)\frac{\partial\Lambda_{f_2}}{\partial f_2'(x)} - \frac{\partial\Gamma_4}{\partial x}\frac{\partial\Lambda_{f_2}}{\partial f_2'(x)}\right]_{x=l_4} = 0 \quad (34)$$

From Eqs. (29) and (32), the general expressions for $f_1(x)$, $f_1'(x)$, $f_2(x)$ and $f_2'(x)$ can be obtained (Eqs. (35)-(38)).

$$f_1'(x) = \sigma_{ci}^{\frac{B-1}{B}}A^{-\frac{1}{B}}B^{-1}\rho^{\frac{1-B}{B}}g_a(t)^{\frac{1-B}{B}}\left[x - c_0\rho^{-1}g_a(t)^{-1}\right]^{\frac{1-B}{B}} \quad (35)$$

$$f_1(x) = \sigma_{ci}^{\frac{B-1}{B}}A^{-\frac{1}{B}}\rho^{\frac{1-B}{B}}g_a(t)^{\frac{1-B}{B}}\left[x - c_0\rho^{-1}g_a(t)^{-1}\right]^{\frac{1}{B}} + c_1 \quad (36)$$

$$f_2'(x) = \sigma_{ci}^{\frac{B-1}{B}}A^{-\frac{1}{B}}B^{-1}\rho^{\frac{1-B}{B}}g_a(t)^{\frac{1-B}{B}}\left[x - c_2\rho^{-1}g_a(t)^{-1}\right]^{\frac{1-B}{B}} \quad (37)$$

$$f_2(x) = \sigma_{ci}^{\frac{B-1}{B}}A^{-\frac{1}{B}}\rho^{\frac{1-B}{B}}g_a(t)^{\frac{1-B}{B}}\left[x - c_2\rho^{-1}g_a(t)^{-1}\right]^{\frac{1}{B}} + c_3 \quad (38)$$

where c_i (i = 0,1,2,3) are unknown integral constants. Combining the geometric relations of Figs. 3(a) and 3(b) with Eqs. (36) and (38), the endpoints of curves $f_1(x)$ and $f_2(x)$ can be expressed as Eqs. (39)-(42).

$$f_1(l_1) = \sigma_{ci}^{\frac{B-1}{B}}A^{-\frac{1}{B}}\rho^{\frac{1-B}{B}}g_a(t)^{\frac{1-B}{B}}\left[l_1 - c_0\rho^{-1}g_a(t)^{-1}\right]^{\frac{1}{B}} + c_1 = 0 \quad (39)$$

$$f_1(l_3) = \sigma_{ci}^{\frac{B-1}{B}}A^{-\frac{1}{B}}\rho^{\frac{1-B}{B}}g_a(t)^{\frac{1-B}{B}}\left[l_3 - c_0\rho^{-1}g_a(t)^{-1}\right]^{\frac{1}{B}} + c_1 = -H\cos^{-1}\theta - \tan\theta(l_1 - l_3) \quad (40)$$

$$f_2(l_2) = \sigma_{ci}^{\frac{B-1}{B}}A^{-\frac{1}{B}}\rho^{\frac{1-B}{B}}g_a(t)^{\frac{1-B}{B}}\left[l_2 - c_2\rho^{-1}g_a(t)^{-1}\right]^{\frac{1}{B}} + c_3 = 0 \quad (41)$$

$$f_2(l_4) = \sigma_{ci}^{\frac{B-1}{B}}A^{-\frac{1}{B}}\rho^{\frac{1-B}{B}}g_a(t)^{\frac{1-B}{B}}\left[l_4 - c_2\rho^{-1}g_a(t)^{-1}\right]^{\frac{1}{B}} + c_3 = -H\cos^{-1}\theta + \tan\theta(l_2 - l_4) \quad (42)$$

Eqs. (39)-(42), combined with Eqs. (35) and (37), are substituted into Eqs. (30), (31), (33) and (34) to obtain expressions for c_1 and c_3 (Eqs. (43)-(46)), respectively.

$$c_{1a} = -(\sigma_t + q)\rho^{-1}g_a(t)^{-1} - \left[2l_1 - l_3 - c_0\rho^{-1}g_a(t)^{-1}\right]\tan\theta \quad (43)$$

$$c_{3a} = -(\sigma_t + q)\rho^{-1}g_a(t)^{-1} + \left[2l_2 - l_4 - c_2\rho^{-1}g_a(t)^{-1}\right]\tan\theta \quad (44)$$

$$c_{1b} = -(\sigma_t + q)\rho^{-1}g_a(t)^{-1} - \left[l_3 - c_0\rho^{-1}g_a(t)^{-1}\right]\tan\theta \quad (45)$$

$$c_{3b} = -(\sigma_t + q)\rho^{-1}g_a(t)^{-1} + \left[l_4 - c_2\rho^{-1}g_a(t)^{-1}\right]\tan\theta \quad (46)$$

where subscripts a and b represent different values of the same parameter in different expressions. Eqs. (19), (39)-(40) and (43) are combined to obtain the values of [l_{1a}, l_{3a}, c_{0a}, c_{1a}] of $f_{1a}(x)$. Similarly, the values of [l_{1b}, l_{3b}, c_{0b}, c_{1b}] of $f_{1b}(x)$, [l_{2a}, l_{4a}, c_{2a}, c_{3a}] of $f_{2a}(x)$ and [l_{2b}, l_{4b}, c_{2b}, c_{3b}] of $f_{2b}(x)$ are obtained. If θ = 0, $f_{1a}(x)$, $f_{1b}(x)$, $f_{2a}(x)$ and $f_{2b}(x)$ will be consistent.

According to the limit analysis theory, collapse is more likely to occur if the collapsing block is separated by a smaller internal energy dissipation rate. Then the expression of the collapse curve can be selected by comparing its internal energy dissipation rate (Eqs. (47) and (48)).

Table 1 The value of the parameters

Parameters	σ_{ci} (MPa)	m_i	GSI	D	ρ (kg/m^3)	υ	H (m)	q (kPa)
Value	10	2.5	55	0.2	2000	0.3	4	10
Parameters	σ_s (kPa)	k_h	k_v	Y (m)	y (m)	f (Hz)	f_k	v_p (m/s)
Value	5	0.2	0.13	50	0	3	1.2	2500

$$f_1(x)=\begin{cases} f_{1a}(x), |\dot{D}_{1a}|<|\dot{D}_{1b}| \\ f_{1b}(x), |\dot{D}_{1a}|>|\dot{D}_{1b}| \end{cases} \quad (47)$$

$$f_2(x)=\begin{cases} f_{2a}(x), |\dot{D}_{2a}|<|\dot{D}_{2b}| \\ f_{2b}(x), |\dot{D}_{2a}|>|\dot{D}_{2b}| \end{cases} \quad (48)$$

where

$$\dot{D}_{1a,b}=\int_{l_{3a,b}}^{l_{1a,b}} w\dot{D}_{i1a,b}\left[1+f_{1a,b}'(x)^2\right]^{\frac{1}{2}}dx \quad (49)$$

$$\dot{D}_{2a,b}=\int_{l_{4a,b}}^{l_{2a,b}} w\dot{D}_{i2a,b}\left[1+f_{2a,b}'(x)^2\right]^{\frac{1}{2}}dx \quad (50)$$

Finally, the collapse curves $f_1(x)$ and $f_2(x)$ are converted into the expressions for $F_1(X_1)$ and $F_2(X_2)$ (Eqs. (51)-(55)).

$$F_1(X_1)=\left[f_1(x)+(l_1-x)\tan\theta\right]\cos\theta,\quad l_3\le x\le l_1 \quad (51)$$

$$X_1=\left[f_1(x)+(l_1-x)\tan\theta\right]\sin\theta+x\cos^{-1}\theta,\quad l_3\le x\le l_1 \quad (52)$$

$$F_2(X_2)=\left[f_2(x)-(l_2-x)\tan\theta\right]\cos\theta,\quad l_4\le x\le l_2 \quad (53)$$

$$X_2=\left[f_2(x)-(l_2-x)\tan\theta\right]\sin\theta-x\cos^{-1}\theta,\quad l_4\le x\le l_2 \quad (54)$$

$$L_i=l_i/\cos\theta,\quad i=1,2,3,4 \quad (55)$$

3. Results and discussions

For results analysis, parameters are defined as Table 1.

Compared with the surface width of the rock block predicted to collapse, the bottom width needs more attention, which limits the safe width of tunnel excavation.

In addition, in order to eliminate the dimensional influence, a dimensionless parameter width-depth ratio L/H is defined, where $L = L_1 + L_2$. This parameter can not only analyze the bottom width of the predicted collapsing rock block, but also study the stability of the overlying rock mass of the tunnel, that is, a large L/H usually indicates strong rock stability. Therefore, in the results analysis, the influences of parameters in Table 1 on L/H are discussed.

3.1 The influence of acceleration parameters

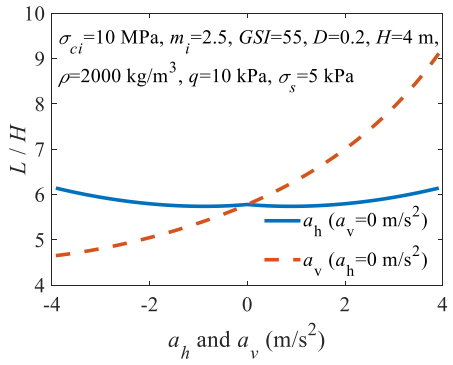

Fig. 4 Effects of acceleration amplitude on width-depth ratio

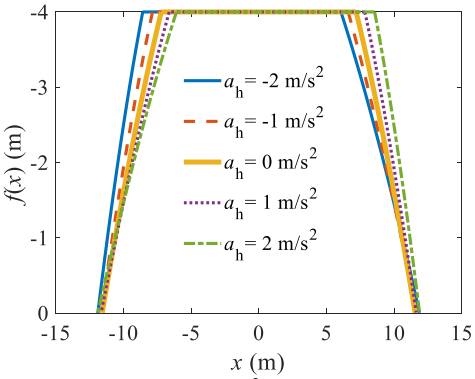

(a) a_h (m/s^2) (a_v = 0)

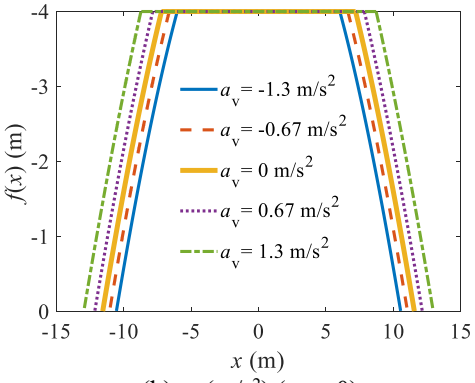

(b) a_v (m/s^2) (a_h = 0)

Fig. 5 The influence of seismic acceleration on the geometry of collapse curve (σ_{ci}=10 MPa, m_i=2.5, GSI =55, D =0.2, ρ=2000 kg/m^3, H =4 m, q =10 kPa, σ_s =5 kPa)

When horizontal and vertical seismic accelerations act on rock mass respectively, the influence curve of L/H is shown in Fig. 4, and the influence on the geometric shape of the collapse curve is shown in Fig. 5. Combined with

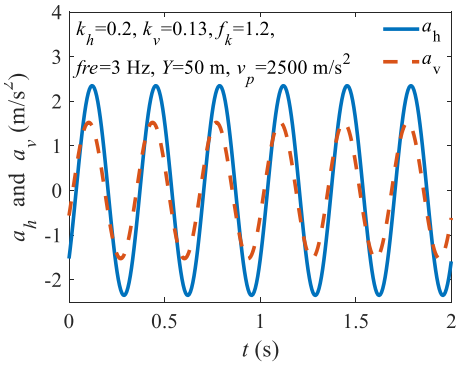

Fig. 6 The variation of horizontal and vertical seismic accelerations with time

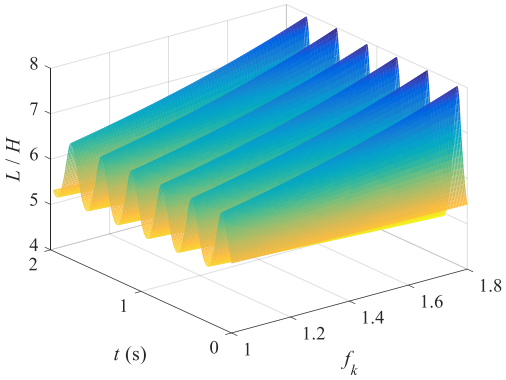

Fig. 8 The influence of amplification factor on width-depth ratio

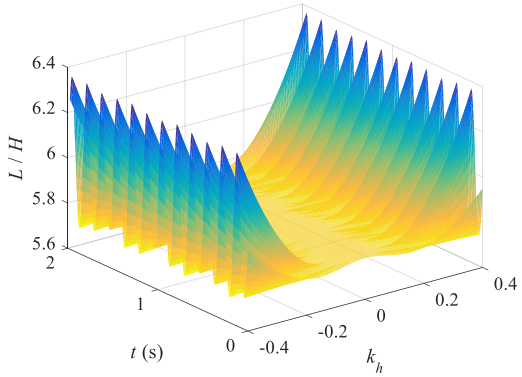

(a) k_h (k_v = 0)

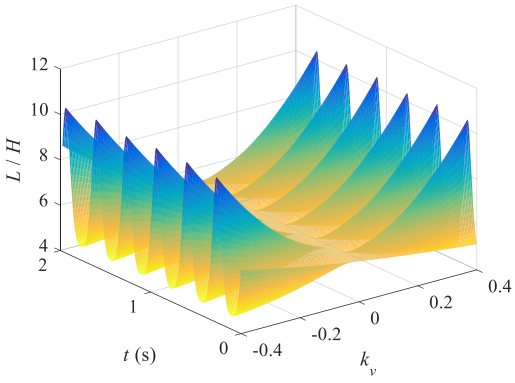

(b) k_v (k_h = 0)

Fig. 7 The influence of acceleration coefficients on width-depth ratio

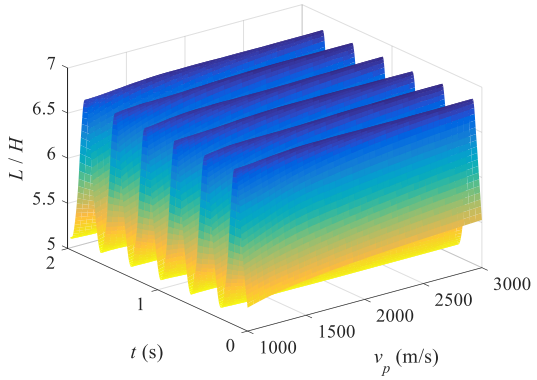

Fig. 9 The influence of longitudinal wave velocity on width-depth ratio

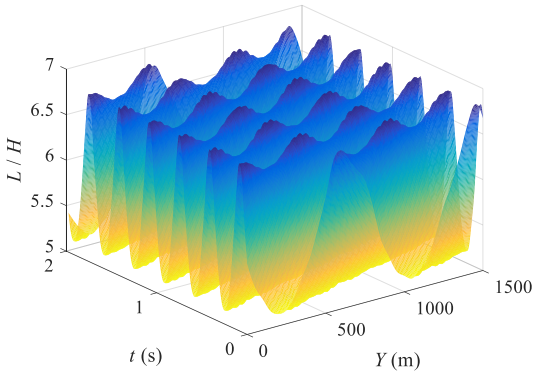

Fig. 10 The influence of rock thickness on width-depth ratio

Figs. 4 and 5(a), it can be seen that the geometric shape of the collapse curve under the action of horizontal seismic acceleration is skewed along the action direction of acceleration and has little influence on L/H. As the main reason of inducing rock collapse is gravity, vertical seismic acceleration acts along gravity direction promote rock collapse, and L/H decreases. Correspondingly, Figs. 4 and 5(b) reflect that the vertical seismic acceleration makes the primary contribution to the width-depth ratio without altering the shape of the collapse curve.

When seismic acceleration is defined as a function of time t, the magnitudes of horizontal and vertical seismic acceleration are shown in Fig. 6. Figs. 7(a) and 7(b) show the influence of horizontal and vertical acceleration coefficients on L/H in time dimension, respectively. It can be found that L/H changes with time, and its amplitude is determined by k_h and k_v, and their influence are consistent with Fig. 4.

When horizontal seismic acceleration and vertical seismic acceleration work together, the influence of seismic amplification factor on L/H is shown in the Fig. 8. As can be seen, the seismic amplification coefficient has a positive correlation effect on the amplitude of L/H. The influence of longitudinal wave velocity on L/H is shown in Fig. 9. The longitudinal wave velocity has a slight influence on the change of L/H in time, but has no influence on the amplitude of L/H.

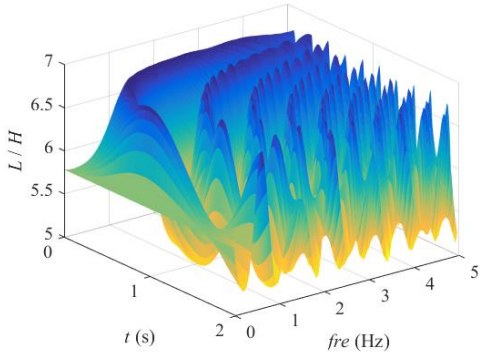

Fig. 11 The influence of seismic wave frequency on width-depth ratio

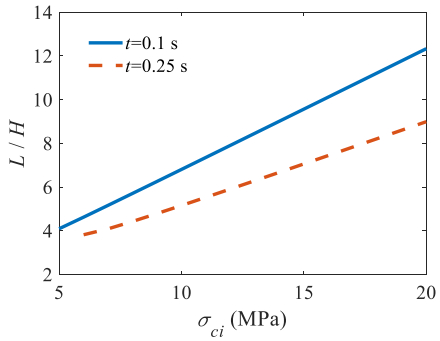

(a) Effects of σ_{ci} on L/H

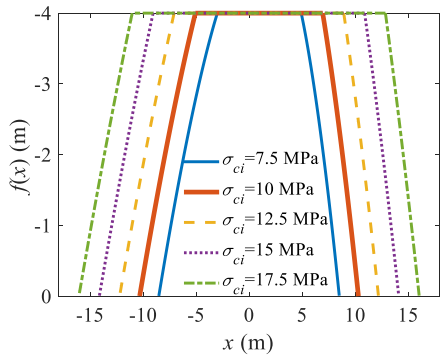

(b) Effects of σ_{ci} on the shape of collapse curves

Fig. 12 The influence of compressive strength σ_{ci} on collapse curves (m_i=2.5, *GSI* =55, D =0.2, ρ=2000 kg/m^3, H =4 m, q =10 kPa, σ_s =5 kPa, k_h=0.2, k_v=0.13, f_k=1.2, *fre*=3 Hz, Y=50 m, v_p=2500 m/s^2, t=0.25 s)

Compared with the longitudinal wave velocity, the thickness of rock strata has a greater influence on the change of L/H in time, and makes the amplitude of L/H change periodically (Fig. 10).

The influence of seismic wave frequency on L/H is shown in Fig. 11. The frequency of seismic wave makes time has a great effect on L/H, but also does not affect the amplitude of L/H.

In general, the parameters k_h, k_v and f_k have a significant effect on the amplitude of L/H because they directly change the amplitude of the acceleration (Figs. 7 and 8). Parameters v_p, Y and f mainly affect the phase difference of seismic acceleration, resulting in no effect on the amplitude of L/H (Figs. 9-11).

3.2 The influence of rock strength parameters

As L/H is mainly affected by vertical acceleration, compared with horizontal seismic acceleration, the maximum and minimum values of vertical acceleration are taken to analyze the rock mass strength parameters. And the vertical seismic acceleration reaches its peak at about t = 0.1 s and t = 0.25 s.

Fig. 12 shows the influence of compressive strength on collapse curves. When the two σ_{ci} - L/H curves at t = 0.1 s and t = 0.25 s are plotted in Fig. 12(a), it means that the results of L/H are always between the two curves as time and compressive strength change. Fig. 12(b) shows the influence of compressive strength on the geometry of the collapse curve, in which it can also be seen that the compressive strength has a great influence on the overall width of the collapsing rock block and almost no influence on the slope of the collapse curve. Compared with Fig. 12, the influence of *GSI* on the collapse curve is similar (Fig. 12(b) and 13(b)), but the influence of *GSI* on L/H is greater (Fig. 12(a) and 13(a)).

The influence of material constant m_i on collapse curves is shown in Fig. 14. Material constant m_i has little influence on L/H (Fig. 14(a)), but has great influence on slope of collapse curve (Fig. 14(b)). A small material constant m_i results in a large slope of the collapse curve, which leads to a small width at the surface of collapsing block.

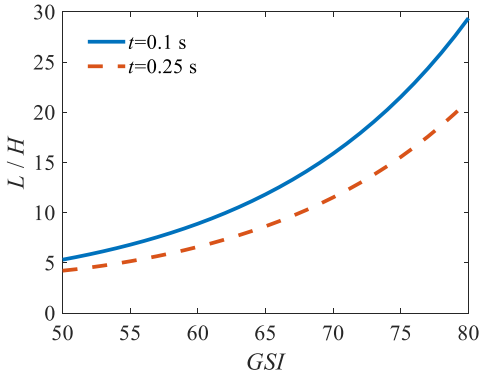

(a) Effects of *GSI* on L/H

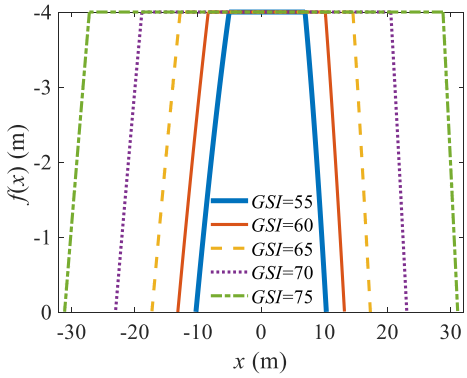

(b) Effects of *GSI* on the shape of collapse curves

Fig. 13 The influence of *GSI* on collapse curves (σ_{ci} =10 MPa, m_i=2.5, D =0.2, ρ=2000 kg/m^3, H =4 m, q =10 kPa, σ_s =5 kPa, k_h=0.2, k_v=0.13, f_k=1.2, *fre*=3 Hz, Y=50 m, v_p=2500 m/s^2, t=0.25 s)

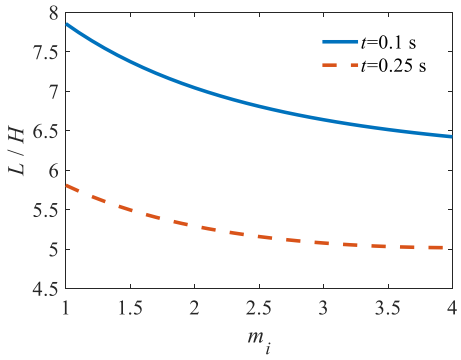

(a) Effects of m_i on L/H

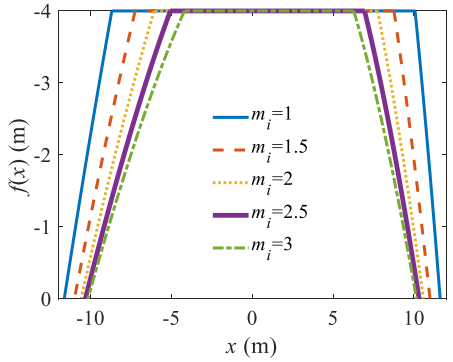

(b) Effects of m_i on the shape of collapse curves

Fig. 14 The influence of material constant m_i on collapse curves (σ_{ci} =10 MPa, *GSI* =55, D =0.2, ρ=2000 kg/m^3, H =4 m, q =10 kPa, σ_s =5 kPa, k_h=0.2, k_v=0.13, f_k=1.2, *fre*=3 Hz, Y=50 m, v_p=2500 m/s^2, t=0.25 s)

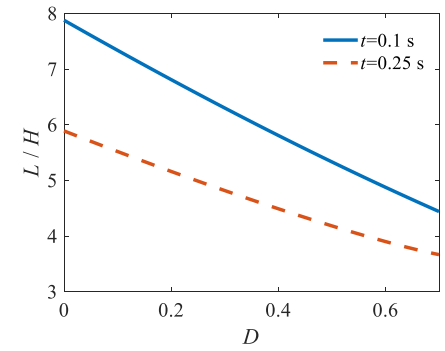

(a) Effects of D on L/H

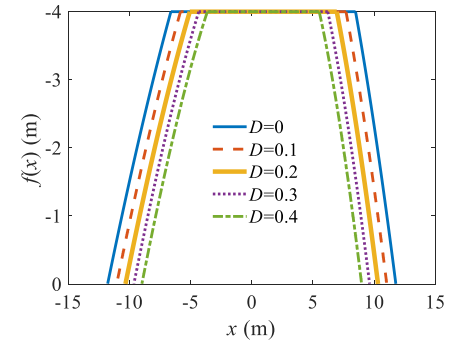

(b) Effects of m_i on the shape of collapse curves

Fig. 15 The influence of D on collapse curves (σ_{ci} =10 MPa, m_i=2.5, *GSI* =55, ρ=2000 kg/m^3, H =4 m, q =10 kPa, σ_s =5 kPa, k_h=0.2, k_v=0.13, f_k=1.2, *fre*=3 Hz, Y=50 m, v_p=2500 m/s^2, t=0.25 s)

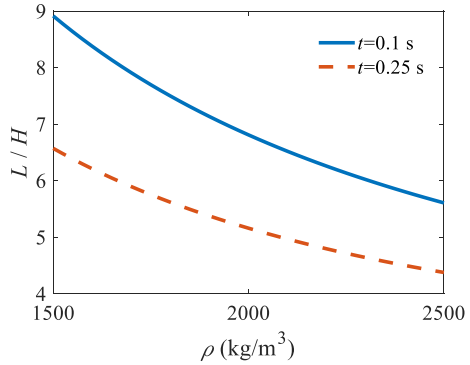

(a) Effects of ρ on L/H

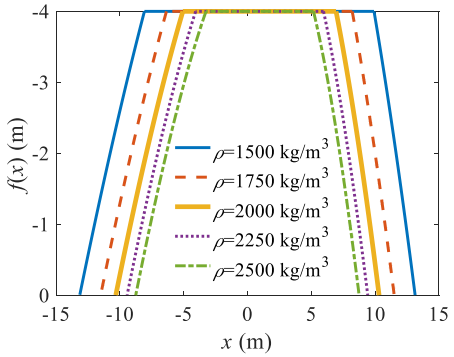

(b) Effects of ρ on the shape of collapse curves

Fig. 16 The influence of ρ on collapse curves (σ_{ci} =10 MPa, m_i=2.5, *GSI* =55, D =0.2, H =4 m, q =10 kPa, σ_s =5 kPa, k_h=0.2, k_v=0.13, f_k=1.2, *fre*=3 Hz, Y=50 m, v_p=2500 m/s^2, t=0.25 s)

In addition, both the disturbance factor D and density ρ have little effect on L/H and have no effect on slope of collapse curves (Fig. 15(b) and 16(b)). In short, the rock mass with strong mechanical properties and light weight has strong stability and large size of collapsing rock block (Figs. 15(a) and 16(a)).

3.3 The influence of the engineering parameters

The influence of the depth of tunnel H on collapse curves is shown in Fig. 17. As shown in Fig. 17(a), L/H decreases with the increase of H, and the change of L/H eventually approaches zero. And it is worth noting that Fig. 17(b) shows that the variation of the width of the collapsing block increases with the increase of H.

Figs. 18 and 19 respectively show the influence of support pressure q and uniformly load σ_s on the collapse curve. Both of them have little effect on L/H (Figs. 18(a) and 19(a)) and have no effect on slope of collapse curve (Figs. 18(b) and 19(b)). In fact, compared with the uniformly load on the surface, the support pressure has a slightly greater impact on L/H.

3.4 Comparative analysis against the horizontal slice method

In previous studies on rock mass collapse, the horizontal slice method based on the Mohr-Coulomb criterion has also

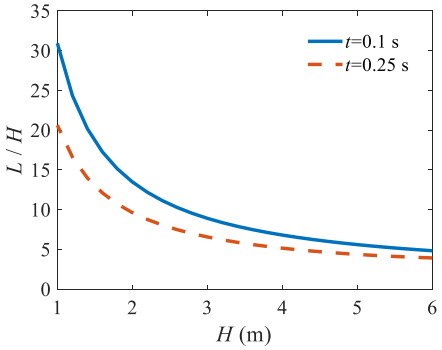

(a) Effects of H on L/H

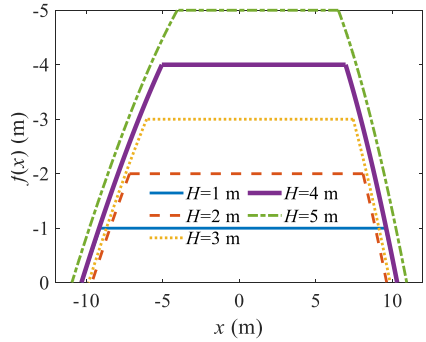

(b) Effects of H on the shape of collapse curves

Fig. 17 The influence of H on collapse curves (σ_{ci} =10 MPa, m_i=2.5, GSI =55, D =0.2, ρ=2000 kg/m^3, q =10 kPa, σ_s =5 kPa, k_h=0.2, k_v=0.13, f_k=1.2, fre=3 Hz, Y=50 m, v_p=2500 m/s^2, t=0.25 s)

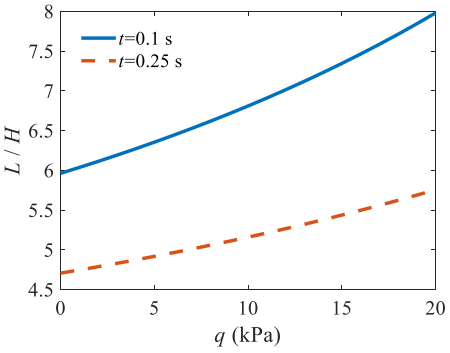

(a) Effects of q on L/H

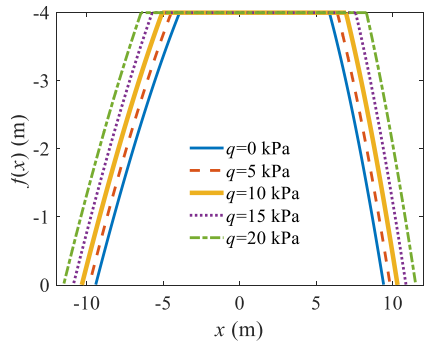

(b) Effects of H on the shape of collapse curves

Fig. 18 The influence of q on collapse curves (σ_{ci} =10 MPa, m_i=2.5, GSI =55, D =0.2, ρ=2000 kg/m^3, H =4 m, σ_s =5 kPa, k_h=0.2, k_v=0.13, f_k=1.2, fre=3 Hz, Y=50 m, v_p=2500 m/s^2, t=0.25 s)

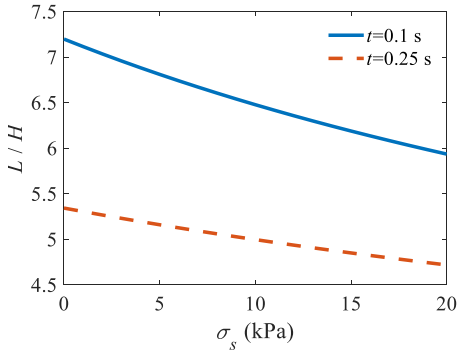

(a) Effects of σ_s on L/H

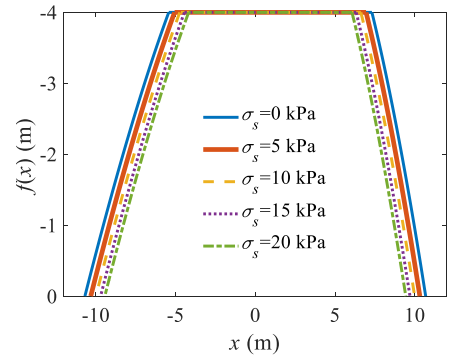

(b) Effects of σ_s on the shape of collapse curves

Fig. 19 The influence of load σ_s on collapse curves (σ_{ci} =10 MPa, m_i=2.5, GSI =55, D =0.2, ρ=2000 kg/m^3, H =4 m, q =10 kPa, k_h=0.2, k_v=0.13, f_k=1.2, fre=3 Hz, Y=50 m, v_p=2500 m/s^2, t=0.25 s)

been applied to address shallow and asymmetric problems (Guo *et al.* 2019). Guo *et al.* (2019) adopted the pseudo-dynamic method to simulate the seismic action, established the safety factor equation of the seismic sliding problem of the overlying rock mass of the circular tunnel, and obtained the shape and position of the sliding surface by calculating its extreme value. Although the collapse block in Guo et al. (2019) is an inverted trapezoid, the method remains applicable to problems with regular trapezoid. Therefore, in a rectangular tunnel, the safety factor k_{sl} equation of linear sliding problem can be written as

$$k_{sl}=\frac{cl+\tan\varphi\cos\beta\begin{bmatrix}W\left(1+k_v\right)+F_h\tan\beta-F_v\\-Wk_h\tan\beta+\sigma_sL_2-qL_1\end{bmatrix}}{\begin{matrix}W\left(1+k_v\right)\sin\beta+Wk_h\cos\beta-F_h\cos\beta\\-F_v\sin\beta+\left(\sigma_sL_2-qL_1\right)\sin\beta\end{matrix}} \tag{56}$$

$$\sin\beta=k\left(1+k^2\right)^{-1/2},\quad \cos\beta=\left(1+k^2\right)^{-1/2} \tag{57}$$

$$L_2=L_1+Hk^{-1},\quad l=H\left(1+k^2\right)^{1/2}k^{-1} \tag{58}$$

where c and φ are the cohesion and friction angle of rock mass, F_h and F_v are the horizontal and vertical forces on the section, β and l are the angle and length of the sliding surface, respectively (Fig. 20).

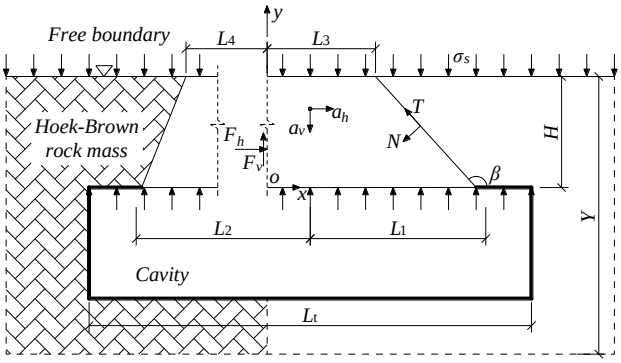

Fig. 20 Linear sliding mechanism of shallow tunnel

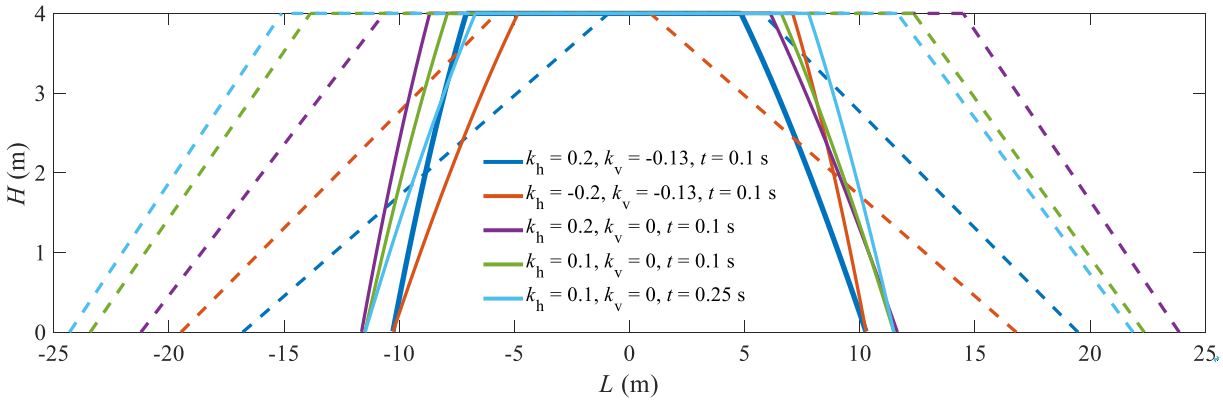

Fig. 21 Comparison of collapse curves between this study (solid line) and the linear sliding mechanism (dashed line) (σ_{ci} =10 MPa, m_i=2.5, *GSI* =55, *D* =0.2, ρ=2000 kg/m^3, *H* =4 m, *q* =10 kPa, σ_s =5 kPa)

Assuming that $F_v = 0$ (Guo *et al.* 2019), then F_h, L_1 and k are three unknowns in Eq. (56). The analytical solution of the sliding surface can be obtained by calculating the extremum problem under the following conditions

$$\partial k_{sl} / \partial L_1 = 0 \tag{59}$$

$$\partial k_{sl} / \partial F_h = 0 \tag{60}$$

The collapse curves obtained by the two methods are shown in Fig. 21. As can be seen from the figure, the slope trend of collapse curves under the action of seismic waves is similar. However, the bottom width L of the collapsing rock block obtained by force balance equation (Eqs. (56) and (61)) is always greater than that obtained by the virtual power equation (Eqs. (23) and (24)). Thus, considering the seismic action, it is safer to use the width of collapsing rock predicted by the method proposed in this study to guide the design of tunnel width.

$$k_{sl} = 1 \tag{61}$$

4. Conclusions

In this paper, the pseudo-dynamic analysis is used to simulate the effect of seismic waves on the overlying rock mass of the shallow tunnel, and an analytical method of asymmetric collapse curve is proposed. The influences of acceleration parameters, rock strength parameters and engineering parameters on the collapse curve are studied. Based on the results, it is found that:

- In the pseudo-dynamic analysis of the overlying rock mass of shallow tunnel, the width of the rock block predicted to collapse will change with time. Therefore, after finding the minimum width of the collapsing rock block, the width of tunnel excavation should be limited within this width to prevent the occurrence of collapse.
- Without considering the damage or strength weakening of rock mass under earthquake, the horizontal seismic acceleration affects the geometry of the rock block predicted to collapse. The vertical seismic acceleration acting downward makes a smaller size of rock block satisfy the collapse condition, that is, the collapse is more likely to occur, while the upward action prevents the collapse.
- The seismic wave parameters (seismic wave amplification coefficient, horizontal seismic coefficient and vertical seismic coefficient) that affect the amplitude of seismic wave will affect the minimum width of the rock block predicted to collapse. The longitudinal wave velocity, thickness of rock strata and frequency only change the phase of seismic wave, but do not change the minimum width of the rock block predicted to collapse.
- The rock mass with strong mechanical properties and light weight has strong stability and large width of predicted

collapse block. The stability of overlying rock mass will be weakened with the increase of tunnel depth, and eventually tend to be stable. The support pressure of the tunnel on the overlying rock mass will enhance the stability of the rock mass, while the uniformly load on the surface will weaken the stability of the rock mass.

Acknowledgments

This research was financially supported by National Key R&D Program of China (No.2022YFC3003601), the National Natural Science Foundation of China (No.51991393), the Key International (Regional) Joint Research Project (No.52020105002) and Guangzhou Science and Technology Program (No.202201020155).

References

Abdelhalim, A., Naggar, M.H.E., Kim, K., Hussein, A.F. and Elgamal, A. (2025), "Seismic performance and soil-structure interaction of shallow reinforced concrete tunnels", *Soil Dyn. Earthq. Eng.*, **194**, 109372. https://doi.org/10.1016/j.soildyn.2025.109372.

Azadi, M., Ghasemi, S.H. and Mohammadi, M. (2020), "Reliability analysis of tunnels with consideration of the earthquakes extreme events", *Geomech. Eng.*, **22**(5), 433-439. https://doi.org/10.12989/gae.2020.22.5.433.

Chen, W.F. (1975), *Limit analysis and soil plasticity*, Elsevier Science, Amsterdam.

Chen, W.F. and Liu, X.L. (1990), *Limit analysis in soil mechanics*, Elsevier Science, Amsterdam.

Choudhury, D. and Nimbalkar, S. (2006), "Pseudo-dynamic approach of seismic active earth Pressure behind retaining wall", *Geotech. Geol. Eng.*, **24**(6), 1103-1113.

Fraldi, M. and Guarracino, F. (2009), "Limit analysis of collapse mechanisms in cavities and tunnels according to the Hoek–Brown failure criterion", *Int. J. Rock Mech. Min. Sci.*, **46**(4), 665-673. https://doi.org/10.1016/j.ijrmms.2008.09.014.

Fraldi, M. and Guarracino, F. (2010), "Analytical solutions for collapse mechanisms in tunnels with arbitrary cross sections", *Int. J. Solids Struct.*, **47**(2), 216-223. https://doi.org/10.1016/j.ijsolstr.2009.09.028.

Fraldi, M. and Guarracino, F. (2011), "Evaluation of impending collapse in circular tunnels by analytical and numerical approaches", *Tunn. Undergr. Sp. Tech.*, **26**(4), 507-516. https://doi.org/10.1016/j.tust.2011.03.003.

Guo, Z., Liu, X., Li, L. and Zhu, Z. (2019), "Seismic analysis of shallow tunnel collapse mechanisms with the horizontal slice method", *J. Eng. Res.*, **7**(4), 18-36.

Guo, Z., Liu, X. and Zhu, Z. (2021), "Limit analysis of seismic collapse for shallow tunnel in inhomogeneous ground", *Geomech. Eng.*, **24**(5), 491-503. https://doi.org/10.12989/gae.2021.24.5.491.

Hoek, E. and Brown, E.T. (1997), "Practical estimates of rock mass strength", *Int. J. Rock Mech. Min. Sci.*, **34**(8), 1165-1186. https://doi.org/10.1016/S1365-1609(97)80069-X.

Hoek, E. and Brown, E.T. (2019), "The Hoek–Brown failure criterion and GSI – 2018 edition", *J. Rock Mech. Geotech. Eng.*, **11**(3), 445-463. https://doi.org/10.1016/j.jrmge.2018.08.001.

Hoek, E., Carranza-Torres, C. and Corkum, B. (2022), "Hoek-Brown failure criterion-2002 edition", *Proceedings of NARMS-Tac*, **1**(1), 267-273.

Huang F., Zhao L.H., Ling T.H. and Yang X.L. (2017), "Rock mass collapse mechanism of concealed karst cave beneath deep tunnel", *Int. J. Rock Mech. Min. Sci.*, **91**, 133-138. https://doi.org/10.1016/j.ijrmms.2016.11.017.

Huang, Q., Zou, J.F. and Qian, Z.H. (2021), "Seismic stability analysis of tunnel face in purely cohesive soil by a pseudo-dynamic approach", *Geomech. Eng.*, **23**(1), 1-13. https://doi.org/10.12989/gae.2020.23.1.001.

Jiang, Y., Wang, C. and Zhao, X. (2010), "Damage assessment of tunnels caused by the 2004 Mid Niigata Prefecture Earthquake using Hayashi's quantification theory type II", *Nat. Hazards*, **53**(3), 425-441. https://doi.org/10.1007/s11069-009-9441-9.

Kwak, C., Yoo, M. and Park, I. (2024), "Dynamic numerical analysis of the effect of tunneling-induced vibration on combined heat and power plant structures under operation", *Geomech. Eng.*, **38**(5), 497-505. https://doi.org/10.12989/gae.2024.38.5.497.

Liang, J.Y., Cui, J., Lu, Y., Li, Y.D. and Shan, Y. (2022a), "Limit analysis of shallow tunnels collapse problem with optimized solution", *Appl Math. Model.*, **109**, 98-116. https://doi.org/10.1016/j.apm.2022.03.044.

Liang, J.Y., Cui, J., Li, Y.D., Shan, Y. and Donà, M. (2022b), "Upper bound analysis of asymmetric collapse mechanism of shallow tunnel under seismic load", *Chinese J. Rock Mech. Eng.*, **41**(1), 2772-2779. https://doi.org/10.13722/j.cnki.jrme.2021.0378.

Lyu, C., Zeng, Z. and Dong, Y. (2019), "Limit analysis of progressive asymmetrical collapse failure of tunnels in inclined rock stratum", *Symmetry*, **11**(7), 904. https://doi.org/10.3390/sym11070904.

Park, D. and Michalowski, R.L. (2019), "Roof stability in deep rock tunnels", *Int. J. Rock Mech. Min. Sci.*, **124**, 104139. https://doi.org/10.1016/j.ijrmms.2019.104139.

Park, D. (2023), "Complementation of analytical solutions for the quantitative roof stability analysis of rock cavities and tunnels", *Int. J. Rock Mech. Min. Sci.*, **170**, 105556. https://doi.org/10.1016/j.ijrmms.2023.105556.

Park, D. (2025), "Most adverse geometry of structural discontinuity on roof collapse in circular rock tunnels", *Tunn. Undergr. Sp. Tech.*, **165**, 106912. https://doi.org/10.1016/j.tust.2025.106912.

Qin, C.B. and Chian, S.C. (2017), "2D and 3D stability analysis of tunnel roof collapse in stratified rock: A kinematic approach", *Int. J. Rock Mech. Min. Sci.*, **100**, 269-277. https://doi.org/10.1016/j.ijrmms.2017.10.027.

Qin, C.B. and Chian, S.C. (2018), "Revisiting crown stability of tunnels deeply buried in non-uniform rock surrounds", *Tunn. Undergr. Sp. Tech.*, **73**, 154-161. https://doi.org/10.1016/j.tust.2017.12.006.

Steedman, R.S. and Zeng, X. (1990), "Influence of phase on calculation of pseudo-static earth pressure on a retaining wall", *Geotechnique*, **40**(1), 103-112. https://doi.org/10.1680/geot.1990.40.1.103.

Suchowerska, A.M., Merifield, R.S., Carter, J.P. and Clausen, J. (2012), "Prediction of underground cavity roof collapse using the Hoek‐Brown failure criterion", *Comput. Geotech.*, **44**, 93-103. https://doi.org/10.1016/j.compgeo.2012.03.014.

Wang, H.T., Wang, L.G., Li, S.C., Wang, Q., Liu, P. and Li, X.J. (2019), "Roof collapse mechanisms for a shallow tunnel in two-layer rock strata incorporating the influence of groundwater", *Eng. Fail Anal.*, **98**, 215-227. https://doi.org/10.1016/j.engfailanal.2019.01.062.

Wang, W.L., Wang, T.T., Su, J.J., Lin, C.H., Seng, C.R. and Huang, T.H. (2001), "Assessment of damage in mountain tunnels due to the Taiwan Chi-Chi earthquake", *Tunn. Undergr. Sp. Tech.*, **16**(3), 133-150. https://doi.org/10.1016/S0886-7798(01)00047-5.

Wang, Z.Z., Gao, B., Jiang, Y.J. and Yuan, S. (2009),

"Investigation and assessment on mountain tunnels and geotechnical damage after the Wenchuan earthquake", *Science in China Series E: Technological Sciences*, **52**(2), 546-558. https://doi.org/10.1007/s11431-009-0054-z.

Xue, Y., Li, X., Li, G., Qiu, D. and Kong, F. (2020), "An analytical model for assessing soft rock tunnel collapse risk and its engineering application", *Geomech. Eng.*, **23**(5), 441-454. https://doi.org/10.12989/gae.2020.23.5.441.

Yang, X.L. and Huang, F. (2011), "Collapse mechanism of shallow tunnel based on nonlinear Hoek–Brown failure criterion", *Tunn. Undergr. Sp. Tech.*, **26**(6), 686-691. https://doi.org/10.1016/j.tust.2011.05.008.

Yang, X.L. and Huang, F. (2013), "Three-dimensional failure mechanism of a rectangular cavity in a Hoek–Brown rock medium", *Int. J. Rock Mech. Min. Sci.*, **61**, 189-195. https://doi.org/10.1016/j.ijrmms.2013.02.014.

Yang, Z., Lai, S.K., Chen, Z., Yang, J., Liu, A. and Fu, J. (2025), "Dynamic analysis of electrically prestressed highly aligned graphene-reinforced dielectric porous arches under large deformation", *Commun. Nonlinear*, **147**, 108876. https://doi.org/10.1016/j.cnsns.2025.108876.

Zhang, B., Wang, X., Zhang, J.S. and Meng, F. (2017), "Three-dimensional limit analysis of seismic stability of tunnel faces with quasi-static method", *Geomech. Eng.*, **13**(2), 301-318. https://doi.org/10.12989/gae.2017.13.2.301.

Zhang, B., Jiang, J., Zhang, D.B. and Liu, Z. (2021), "Upper bound solution of collapse pressure and permanent displacement of 3D tunnel faces using the pseudo-dynamic method and the kinematic approach", *Geomech. Eng.*, **25**(6), 521-533. https://doi.org/10.12989/gae.2021.25.6.521.

Zhang, X., Jiang, Y. and Maegawa, K. (2020), "Mountain tunnel under earthquake force: A review of possible causes of damages and restoration methods", *J. Rock Mech. Geotech. Eng*., **12**(2), 414-426. https://doi.org/10.1016/j.jrmge.2019.11.002.

Zhu, J., Kontoe, S., Li, X., Liang, J. and Chen, S. (2024), "Ground motion amplification by twin circular tunnels for obliquely incident seismic waves: Effects of saturated poroelastic soil parameters", *Soil Dyn. Earthq. Eng*., **186**, 108953. https://doi.org/10.1016/j.soildyn.2024.108953.

CC

Appendix A. Conversion between the Hoek–Brown criterion and the Mohr envelope

Within the derivation framework of the classical Hoek-Brown failure criterion (Hoek *et al.* 1997), the normal and shear stresses are derived from the principal effective stresses

$$\sigma_n = \sigma_3' + \frac{\sigma_1' - \sigma_3'}{\partial\sigma_1'/\partial\sigma_3' + 1} \tag{A1}$$

$$\tau = (\sigma_1' - \sigma_3')\sqrt{\partial\sigma_1'/\partial\sigma_3'} \tag{A2}$$

If GSI > 25

$$a = 0.5,\ \frac{\partial\sigma_1'}{\partial\sigma_3'} = 1 + \frac{m_b\sigma_{ci}}{2(\sigma_1' - \sigma_3')} \tag{A3}$$

else

$$s = 0,\ \frac{\partial\sigma_1'}{\partial\sigma_3'} = 1 + am_b^a\left(\frac{\sigma_3'}{\sigma_{ci}}\right)^{a-1} \tag{A4}$$

The tensile strength of the rock mass is given by

$$\sigma_t = \frac{\sigma_{ci}}{2}\left(m_b - \sqrt{m_b^2 + 4s}\right) \tag{A5}$$

The equivalent Mohr-Coulomb envelope can be written as

$$Y = \log A + BX$$

$$Y = \log\frac{\tau}{\sigma_{ci}},\ X = \log\frac{(\sigma_n - \sigma_t)}{\sigma_{ci}} \tag{A6}$$

List of Notation

Symbol	Unit	Parameters
σ_1	MPa	Maximum stresses at failure
σ_3	MPa	Minimum stresses at failure
σ_{ci}	MPa	Uniaxial compressive strength of the intact rock pieces
σ_t	MPa	Tensile strength of the rock mass
σ_n	MPa	Normal stress at failure
σ_{ij}	MPa	Any set of stresses of deformations
τ_n	MPa	Shear stress at failure
$\mathfrak{I}$	MPa	Plastic potential
$\dot{\varepsilon}_{ij}^*$	s^{-1}	Any set of strain rate of deformations
$\dot{\varepsilon}_n$	s^{-1}	Normal plastic strain rate
$\dot{\gamma}_n$	s^{-1}	Shear plastic strain rate
t	s	Time
G	kPa	Shear modulus
θ	degree	The angle between the resultant acceleration and the *y*-axis
α	degree	Angle between the tangential direction of the collapse curves and the *x*-axis
β	degree	Angle between the linear sliding surface and the *x*-axis
T_i	N	External forces on the surface
F_i	N	Body forces
$\dot{D}_i$	$N/(m^2\cdot s)$	Rate of dissipation density of the internal forces
$\dot{D}$	N/s	Rate of total dissipation of the internal forces
$\dot{W}$	N/s	Total gravitational potential energy power
$\dot{P}_q$	N/s	Power of support pressure
$\dot{P}_{\sigma_s}$	N/s	Power of uniformly load on the surface
$\dot{\Psi}$	N/s	Rate of total dissipation
q	N/m^2	Support pressure at the bottom of the rock mass
σ_s	N/m^2	Uniformly load on the surface
γ	N/m^3	Weight per unit volume of the rock mass
ρ	kg/m^3	Density
$g_a(t)$	m/s^2	Resultant acceleration
$a_h(t)$	m/s^2	Horizontal seismic acceleration
$a_v(t)$	m/s^2	Vertical seismic acceleration
g	m/s^2	Acceleration of gravity
v_i^*	m/s	Virtual velocity of kinematically admissible velocity field
v	m/s	Velocity of collapsing block
v_s	m/s	Velocity of shear wave
v_p	m/s	Velocity of longitudinal wave
S	m^2	Surfaces of external forces
V	m^3	Volume of the body
$f_1(x)$	m	Collapse curve function of coordinate xo_1y
$f_2(x)$	m	Collapse curve function of coordinate xo_2y
$F_1(X)$, $F_2(X)$	m	Collapse curves function of coordinate xoy
l_1, l_3	m	Distance from the endpoint of curve to the *y*-axis in coordinate xo_1y
l_2, l_4	m	Distance from the endpoint of curve to the *y*-axis in coordinate xo_2y
L_1, L_2,	m	Distance from the endpoint of curve to the

L_3, L_4		y-axis in coordinate xoy
L	m	Width of the bottom of collapsing block
l	m	Length of the linear sliding surface
Y	m	Thickness of the rock stratum
H	m	Depth of tunnel
w	m	Thickness of the plastic deformation region
f	Hz	Frequency
ω	rad/s	Angular frequency
υ	N/A	Poisson's ratio
f_k	N/A	Amplification factor
k_h, k_v	N/A	Coefficients of horizontal and vertical acceleration
m_b, m_i, s, a, A, B	N/A	Material constants
λ	N/A	Scalar parameter
c_0, c_1, c_2, c_3	N/A	Integration constants
c	MPa	Cohesion of rock mass
φ	degree	Friction angle of rock mass
F_v, F_h	N	Horizontal and vertical forces on the section
k_{sl}	N/A	Safety factor